Evaluating the microstructure of human brain tissues using synchrotron radiation-based micro computed tomography

Georg Schulz*[a], Anne Morel[b], Martha S. Imholz[a], Hans Deyhle[a], Timm Weitkamp[c], Irene Zanette[c], Franz Pfeiffer[d], Christian David[e], Magdalena Müller-Gerbl[f], and Bert Müller[a]
[a]Biomaterials Science Center, University of Basel, Basel, Switzerland;
[b]Center for Clinical Research, University Hospital Zurich, Zurich, Switzerland;
[c]European Synchrotron Radiation Facility (ESRF), Grenoble, France;
[d]Department of Physics/Biophysics (E17), Technische Universität München, Garching, Germany;
[e]Laboratory for Micro- and Nanotechnology, Paul Scherrer Institut, Villigen, Switzerland;
[f]Institute of Anatomy, University of Basel, Basel, Switzerland;

ABSTRACT

Minimally invasive deep brain neurosurgical interventions require a profound knowledge of the morphology of the human brain. Generic brain atlases are based on histology including multiple preparation steps during the sectioning and staining. In order to correct the distortions induced in the anisotropic, inhomogeneous soft matter and therefore improve the accuracy of brain atlases, a non-destructive 3D imaging technique with the required spatial and density resolution is of great significance. Micro computed tomography provides true micrometer resolution. The application to post mortem human brain, however, is questionable because the differences of the components concerning X-ray absorption are weak. Therefore, magnetic resonance tomography has become the method of choice for three-dimensional imaging of human brain. Because the spatial resolution of this method is limited, an alternative has to be found for the three-dimensional imaging of cellular microstructures within the brain. Therefore, the present study relies on the synchrotron radiation-based micro computed tomography in the recently developed grating-based phase contrast mode. Using data acquired at the beamline ID 19 (ESRF, Grenoble, France) we demonstrate that grating-based tomography yields premium images of human thalamus, which can be used for the correction of histological distortions by 3D non-rigid registration.

Keywords: X-ray phase contrast, X-ray grating interferometry, X-ray Talbot interferometry, human brain tissue, human thalamus, histology, stereotactic brain atlas

1. INTRODUCTION

The performance of minimally invasive interventions such as gamma knife or MR-guided focused ultrasound surgeries for the treatment of chronic neuropathic pain or movement disorders [1] requires a profound knowledge of the location of the target volume. So far, neurosurgeons use detailed stereotactic atlases of the human thalamus [2,3] for the orientation within the treated part. Such brain atlases are based on histological sectioning with thicknesses of several dozen micrometers. Micrographs on sub-micrometer level of the differently stained histological slices can then be obtained by optical microscopy.

For anisotropic and inhomogeneous soft matter like brain tissue, the multiple preparation steps during sectioning and staining induce local deformations, which are already quantified in two dimensions (2D) using synchrotron-radiation-based micro computed tomography in absorption contrast mode [4]. Here, the histological slices with a lateral spatial resolution better than a micrometer were non-rigidly registered with the less detailed tomography data. The relatively weak contrast in the X-ray tomography data was sufficient [5] to reasonably correct the histological slices and to demonstrate differences between staining protocols. Unfortunately, this study was restricted to corrections in 2D. Three-dimensional (3D), non-destructive techniques for the correction of these spatial distortions with a spatial resolution down to the micrometer level would give even more reliable results and, therefore, would contribute to a more precise generic atlas of the brain parts of interest.

*georg.schulz@unibas.ch; phone +41 61 265 9618; fax +41 61 265 9699; www.bmc.unibas.ch

Developments in X-Ray Tomography VII, edited by Stuart R. Stock, Proc. of SPIE Vol. 7804, 78040F · © 2010 SPIE · CCC code: 0277-786X/10/$18 · doi: 10.1117/12.859273

Magnetic resonance imaging (MRI) is a non-destructive 3D imaging technique with high contrast between white and gray matter. Unfortunately, the limited spatial resolution of around three magnitudes larger than that of the micrographs inhibits the evaluation of the deformation field. Synchrotron radiation-based micro computed tomography (SRμCT) in absorption contrast provides the required spatial resolution. The contrast in the human rostral medulla oblongata was already weak, so that considerable doubt remains as to whether the density resolution in absorption contrast mode actually results in high-quality images of the human thalamus which represents a major challenge in X-ray tomography as it exhibits weak absorption contrast. On this account, the SRμCT experiment was carried out in phase contrast mode which is based on the phase shifts of X-ray waves penetrating the specimen [6]. An overview of the operating modes of the main X-ray phase contrast approaches can be found in literature [7]. During the present study, the recently developed grating interferometry [8-11] was used for the evaluation of the 3D deformation tensor induced by sectioning and staining of the human thalamus and consequently for the correction of the histological slices.

2. MATERIALS AND METHODS

2.1 Preparation of the brain specimen

The specimen was extracted from a donated male body. All procedures were conducted in accordance with the Declaration of Helsinki and according to the ethical guidelines of the Canton of Basel. One day after natural death, the brain was extracted at the Institute of Anatomy (University of Basel, Switzerland) and subsequently transferred to 10% formalin solution for fixation. After two weeks of fixation, a block of the thalamus was obtained by guillotine section at the University Hospital Zurich [3], Switzerland and placed in a container filled with 4% formalin solution. The position of the thalamus within the brain is shown by the MR-derived image in Figure 1. The size of the thalamic block was about $3 \times 3 \times 3$ cm^3.

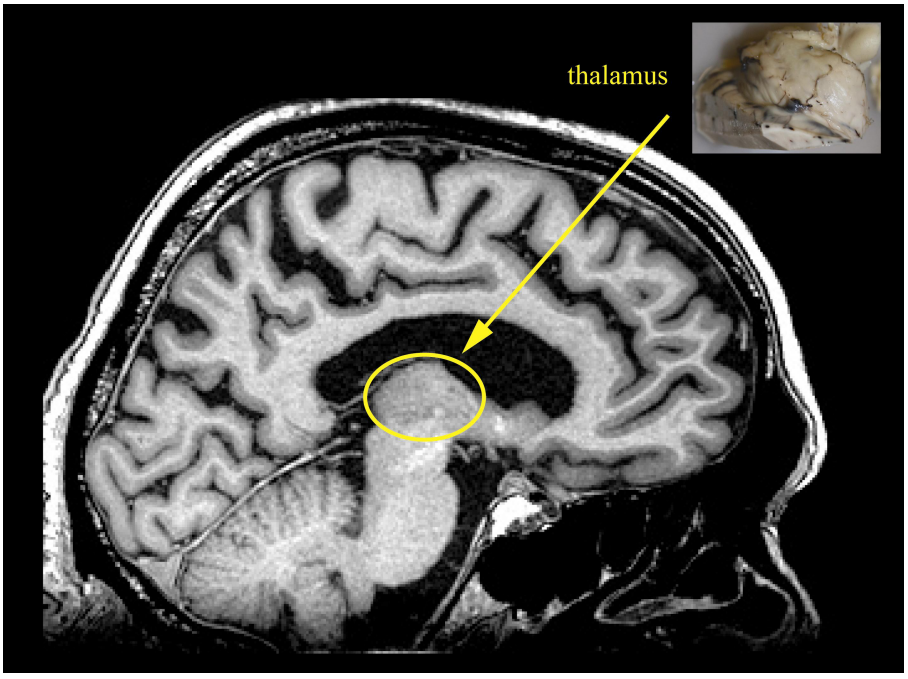

Figure 1. The MRI-slice of the investigated brain and the photography of the extracted thalamus (inset) indicate the location of the specimen inside the brain.

2.2 Grating interferometry

Phase contrast tomography provides information about the three-dimensional distribution of the real part of the refractive index of an object, often expressed in terms of its decrement from unity $\delta(x,y,z)$. Using the relation

$$\delta(x,y,z) = \frac{r_e \lambda^2}{2\pi} \rho_e(x,y,z), \quad (1)$$

where the constant r_e is the classical electron radius, it also yields the electron density distribution $\rho(x,y,z)$ for X-ray energies far away from the absorption edges. During our investigation a grating interferometer was used for detection of $\delta(x,y,z)$. Using the phase-stepping method, it is possible to detect slight deflections of the incoming X-rays caused by the phase object. The relation between local beam propagation direction $\alpha(y,z)$, wave phase shift $\Phi(y,z)$ and decrement of X-ray refractive index $\delta(x,y,z)$ is

$$\alpha(y,z) = \frac{\lambda}{2\pi}\frac{\partial\Phi(y,z)}{\partial y} = \int_{-\infty}^{\infty}\frac{\partial\delta(x,y,z)}{\partial y}dx\,. \tag{2}$$

A detailed description of grating interferometry and in particular of the phase-stepping method was published previously [10,12].

The grating interferometry experiment was performed at the beamline ID 19 (ESRF, Grenoble, France) [13]. The photon energy of 26 keV was selected using a double-crystal Si(111) monochromator in BRAGG geometry. The grating interferometer consists of a beam-splitter grating g_1 with a periodicity of $p_1 \approx 3.99$ µm and a Si structure height of 34 µm, and the analyzer grating g_2 with a periodicity of $p_2 \approx 2$ µm and a structure height of 25 µm. The beam-splitter and the analyzer grating were fabricated at the Paul Scherrer Institut (Villigen, Switzerland) [14]. With a distance between source and interferometer of 150 m and a distance between the gratings of $d \approx 376$ mm (9^{th} Talbot order), the ratio of the grating periods, p_2/p_1, was matched to the beam divergence [15].

The Eppendorf container with the thalamus in formalin solution was fixed at the high-precision rotation stage and immersed in a water tank with parallel polymethylmethacrylat plates for the measurements fixed during the whole experiment. This arrangement ensured minimized artifacts owing to X-ray phase curvature induced by the container surface. Specimen and tank were located about 10 cm upstream of the beam-splitter grating. The detector, placed about 3 cm downstream of the analyzer grating, was a lens-coupled scintillator and charge-coupled device (CCD) system using a FReLoN 2K (Fast-Readout, Low-Noise, ESRF Grenoble, France) CCD with 2048 × 2048 pixels. The effective pixel size corresponded to 31 µm. The field of view was 20.2 mm wide and 12.5 mm high. As the specimen width was larger than the field of view, one experiment was performed with an asymmetric axis position, shifted by 9 mm from the center of the detection unit as used previously [16]. In order to image the entire thalamus, four scans each at different height position of the specimen were acquired. During the second experiment, the axis position was shifted back to the centre of the detection unit and three scans at different height positions were acquired in order to image the inner part of the thalamus in local tomography mode. Projection radiographs were taken in 1200 steps over a range of 360° during the 'off-axis' experiment and 799 steps over a range of 360° during the conventional experiment where the axis position was at the centre of the detection unit. At each projection angle, four phase-stepping images were taken over one period of the interferometer fringe pattern. The exposure time for each image was set to a period of 1 s.

2.3 Histology

After the SRµCT experiments, the block was transferred in progressively increasing sucrose concentrations over around two weeks for cryo-protection. The block was then frozen by immersion in isopentane (~ -30°C) and stored at -75°C. Using a Leica CM 3050, cryostat sections, 50 µm thick, were collected in 0.1 M phosphate buffer. For the staining procedure, the sections were mounted on gelatinized slides and stained for Nissl with cresyl violet or for myelin with a modified Heidenhain procedure [3]. The sections were then recorded (HP scanjet 7400c). Microphotographs of selected thalamic areas were taken using a Leica MZ16 microscope and DFC420-C digital camera.

2.4 Data treatment

After processing of the projections of the 'off-axis' scan, the missing part of each projection was added by the appropriate, 180° shifted projection multiplied by (-1). Both projection datasets were then reconstructed using a modified filter kernel (Hilbert transform) in combination with standard filtered back-projection algorithm [11,17,18].

In order to combine the global 'off-axis' with the local 'non-off-axis' volume, the datasets were registered using a three-dimensional rigid algorithm [19,20] with six degrees of freedom, namely three translation and three rotation degrees. The registration was performed using the classical maximization of mutual information (MI) principle [21,22].

The histological images were stacked to a 3D dataset by approximately correlating the orientations and positions of the slices. For the calculation of the deformation field the tomography and the histological 3D dataset were then registered

using a three-dimensional non-rigid classical maximization of MI algorithm [19]. All the data treatment steps, except the registration, were done with Matlab 7.8 (MathWorks, Natick, USA).

3. RESULTS AND DISCUSSION

Brain tissue provides quite weak X-ray attenuation contrast, which is necessary to distinguish between the grey and white matter or even between grey matter structures such as the nuclei in the thalamus. Therefore, one alternatively uses phase contrast imaging, which possesses much better contrast for soft tissues than absorption contrast.

3.1 Morphology of the human thalamus

The morphology of the thalamus can be investigated by using different staining procedures. Depending on the staining, certain intra- and extra- thalamic structures can be identified. The Haidenhain procedure, for example, shows location of myelinated fiber tracts (or white matter) which are responsible for fast transfer of the impulses. The right image of Figure 2 shows such a myelin-stained section through the posterior part of the human thalamus. The darkness of the color of the slice correlates with the concentration of the myelin. On the basis of this staining, one can differentiate at least between eleven different structures, most of them located outside the human thalamus. The structures belonging to the thalamus are the *reticular thalamic nucleus* (R), the *lateral* and *medial pulvinar* (PuL and PuM) and the *lateral* and *medial geniculate nucleus* (LGN and MGN). Structures belonging to the adjacent tissue are the *putamen* (PuT), the *internal capsule* (ic), the *medial lemniscus* (ml), the *superior colliculus* (SC), the *comissure of the SC* (csc), as well as the *periaqueductal grey area* (PAG).

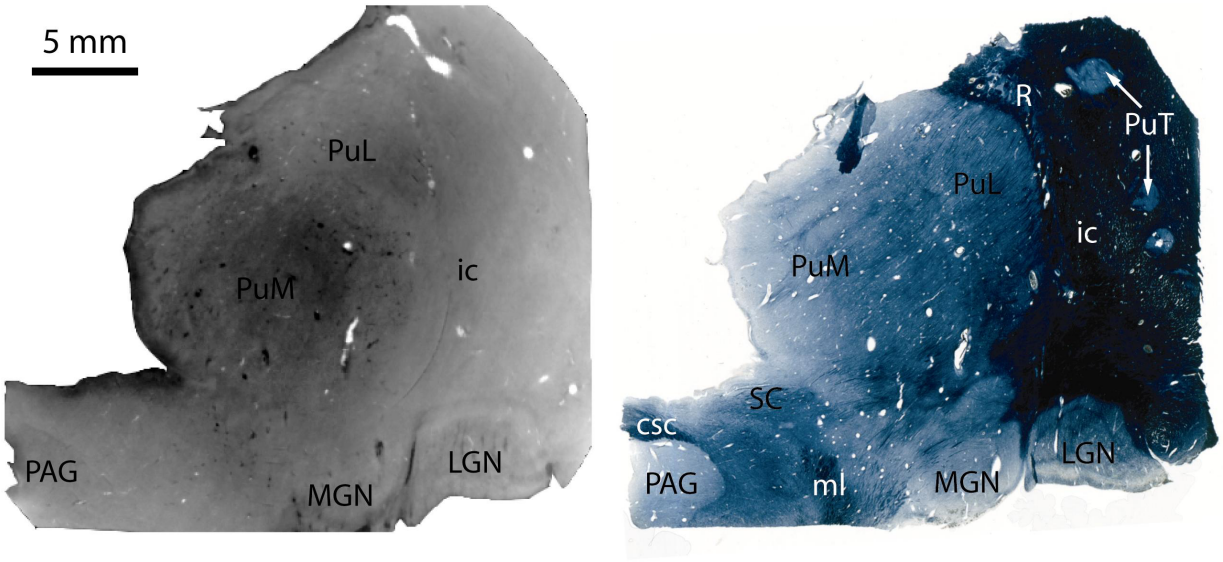

Figure 2. One grating-based SRμCT-slice and the corresponding frontal myelin-stained histological slice. The blue-colored regions correspond to fiber tracts, which contain myelin. A comparison between the tomography and histology data points out, that besides all the blood vessels more than the half of the structures visible on the histological slice can also be identified in the corresponding tomogram.

Another procedure, the Nissl-staining using cresyl violet, allows differentiation of grey nuclei on the basis of cyto-architectonic characteristics in terms of cell sizes and densities. Such Nissl-stained sections of the thalamus are shown on the right hand side of Figure 3. The two sections are located around 1.4 and 0.8 (upper and lower right) cm anterior to the level shown in Figure 2. During this procedure, the cells adopt a blue color as seen in the zoom in of Figure 3. There, the blue-colored structures correspond to individual cells. Therefore, on these low-power images, the intensity of the blue color is mostly related to the cell density. Besides the structures visible in Figure 2, additional nuclei or fiber tracts can be identified at these more anterior levels: the *anteroventral nucleus* (AV), the *mediodorsal nucleus* (MD), the *ventral lateral nucleus* (VL), the *ventral anterior nucleus* (VA), the *zona incerta* (ZI), the *subthalamic nucleus* (STh), the *globus pallidus*, *internal* (GPi) and *external* (GPe) segments, the *optic tract* (ot), the *lateral dorsal nucleus* (LD), the *stria*

medullaris (sm), the *central lateral nucleus* (CL), the *centromedian nucleus* (CM), the *parafascicular nucleus* (Pf), the *red nucleus* (RN), the *fasciculus cerebello-thalamicus* (fct) and the *ventral posterior lateral nucleus* (VPL).

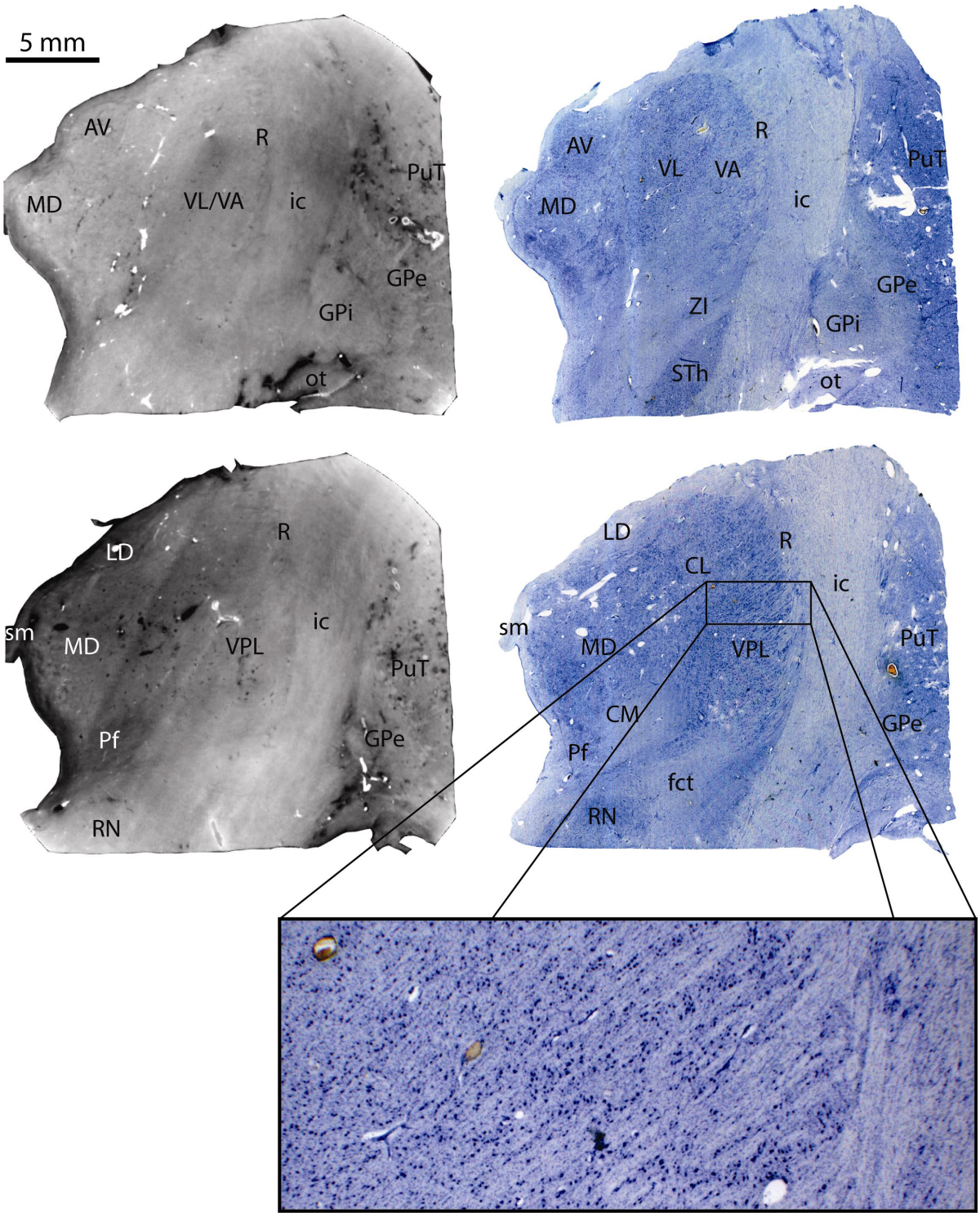

Figure 3. A comparison between the phase contrast and Nissl stained slices shows that also here most of the structures seen in the histology can be identified in the tomograms. With the Nissl, the cells are stained in blue as can be seen in the inset at higher magnification.

As already mentioned, the disadvantages of the histology are the multiple preparation steps which make this technique time consuming and which induce unknown changes in the anisotropic and inhomogeneous tissues like it is the case for brain tissue. According to the selected histological slices, tomograms of the grating-based phase contrast results can be seen on the left hand side of the Figures 2 and 3. With the aid of the histological slices many of the structures can be identified in the phase contrast results. The benefit of this non-destructive imaging technique is that the form and position of the structures are not modified. Another advantage of the tomography results is the isotropic pixel size. For this reason the spatial resolution in the horizontal and sagittal direction of the thalamus illustrated in Figure 4 is even better than that of the present histological data set. Of course, the results of histological sections in the horizontal or sagittal plane would again be better than the tomograms. However, histology results in high quality outcome in only two dimensions. The spatial resolution of the third dimension is always a few magnitudes larger than that of the other two dimensions. Here, the structures can even be better identified than on the frontal tomograms. Besides the already specified structures one can distinguish the *mammillothalamic tract* (mtt), the *fornix* (fx), *posterior commissure* (pc), the *supragenicular nucleus / posterior nucleus* complex (SG/Po), the *superior colliculus* (SC), the *habenular nucleus* (Hb), the *caudate nucleus* (Cd) and the *fasciculus thalamicus* (ft).

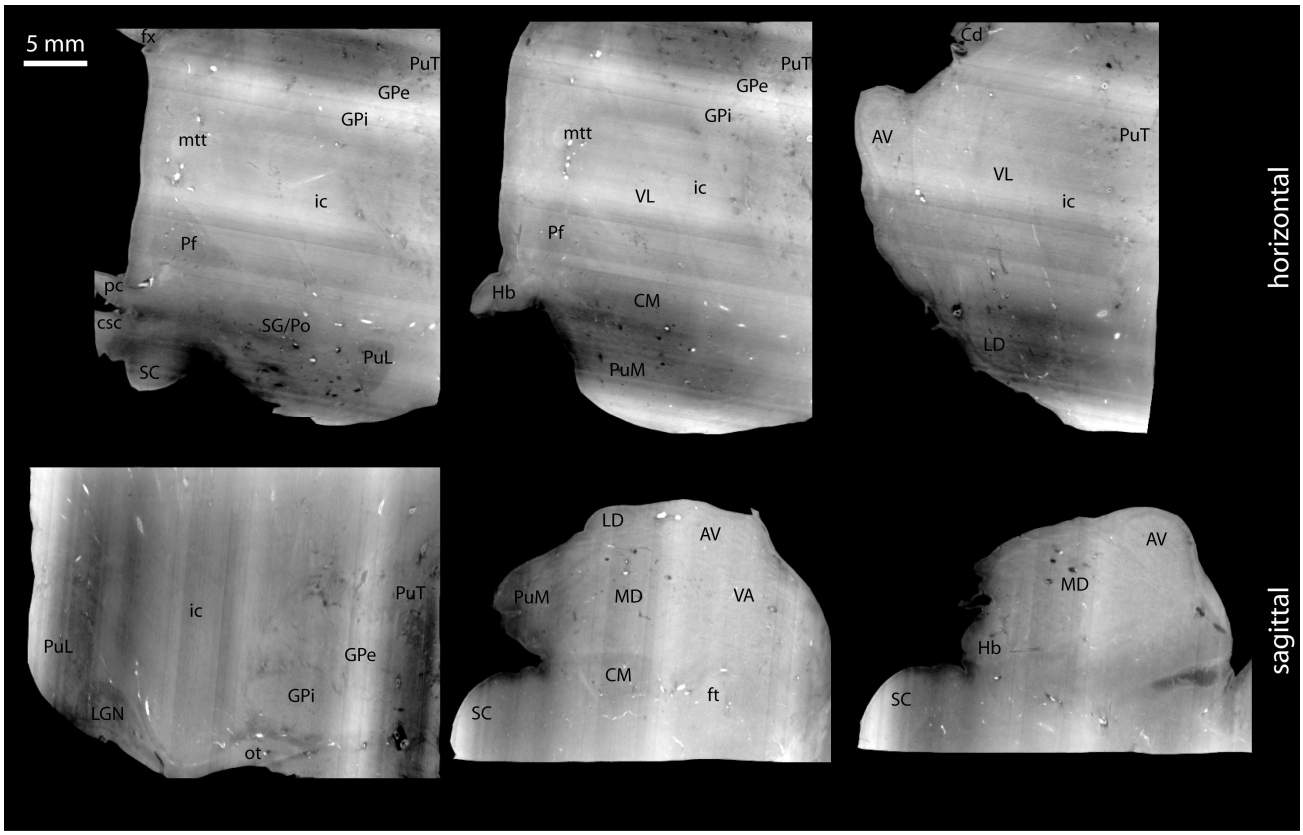

Figure 4. The horizontal and sagittal views of the grating interferometry even more illustrate the possibility to differentiate between different structures inside and outside the thalamus.

3.2 Internal strain field induced by sectioning and Nissl staining

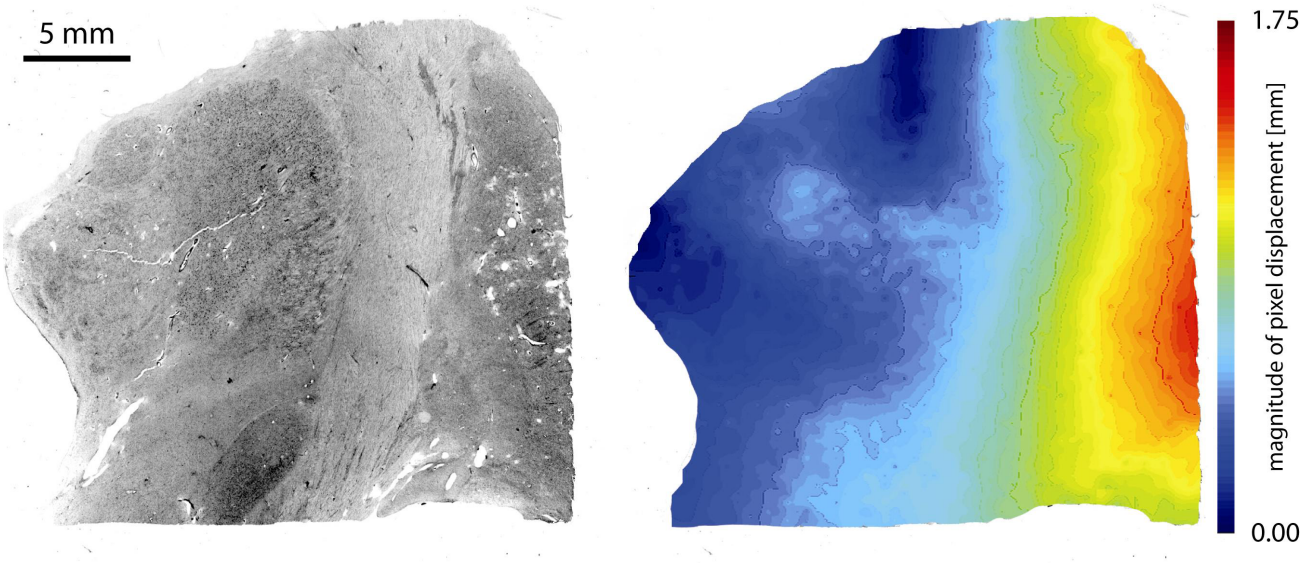

Figure 5. One Nissl-stained histological slice converted to gray scale for the non-rigid registration. The right image shows the corresponding magnitude of the deformation field caused by sectioning and staining.

For the determination of the deformation field, the Nissl-stained sections converted to gray scale were non-rigidly registered. Figure 5 shows one selected slice and the corresponding contribution of the magnitude of the pixel displacements caused during the histological preparation steps. The maximal displacement of this slice amounts to 1.75 mm what corresponds to 5 % of the slice extension. These maximal strain values are found mainly outside the thalamus, at the level of the *putamen* and the *globus pallidus*, most probably to due to large number of blood vessels in this area. The magnitude of the displacements of the internal capsule is around 0.8 mm whereas the strains inside the thalamus are smaller than that value.

4. CONCLUSIONS

Grating-based phase contrast SRμCT is eminently suited for the imaging of human brain tissue with micrometer resolution. The high-quality images of the human thalamus can be used to determine the 3D deformation vector field, which is induced by sectioning and staining during histology and to improve the histological data. Therewith, the corrected histological slices with sub-micrometer resolution should improve the accuracy of stereotactic brain atlases, which can be used for non-invasive MR-guided neurosurgery without intra-cerebral penetration such as with gamma knife or high-intensity focused ultrasounds.

ACKNOWLEDGEMENTS

The authors gratefully acknowledge P. Zimmermann (Basel) for the extraction of the human brain, K. Scheffler and H. Crooijmans (Basel) for the MRI measurements of the brain and A. Andronache (Zurich) for availability of the non-rigid registration tool. The project was partially funded by Swiss National Science Foundation (CR23I2_125 406) and was supported by beam time from the ESRF (proposal MD-328).

REFERENCES

[1] Martin, E., Jeanmonod, D., Morel, A., Zadicario, E. and Werner, B., "High-Intensity Focused Ultrasound for Noninvasive Functional Neurosurgery," Ann. Neurol. 66, 858-861 (2009).

[2] Schaltenbrand, G. and Wahren, W., [Atlas for Stereotaxy of the Human Brain], Thieme, Stuttgart, (1977).

[3] Morel, A., [Stereotactic atlas of the human thalamus and basal ganglia], Informa Healthcare, New York, (2007).

[4] Germann, M., Morel, A., Beckmann, F., Andronache, A., Jeanmonod, D. and Müller, B., "Strain fields in histological slices of brain tissue determined by synchrotron radiation-based micro computed tomography," J. Neurosci. Methods 170(1), 149-155 (2008).

[5] Brooks, R.A., Di Chiro, G. and Keller, M.R., "Explanation of Cerebral White - Gray Contrast in Computed Tomography," J. Comput. Assist. Tomogr. 4(4), 489-491 (1980).

[6] Fitzgerald, R., "Phase-Sensitive X-Ray Imaging," Phys. Tod. 53(7), 23-26 (2000).

[7] Schulz, G., Weitkamp, T., Zanette, I., Pfeiffer, F., Beckmann, F., David, C., Rutishauser, S., Reznikova, E. and Müller, B., "High-resolution tomographic imaging of a human cerebellum: comparison of absorption and grating-based phase contrast," J. R. Soc. Interface, in press (2010).

[8] David, C., Nöhammer, B., Solak, H.H. and Ziegler, E., "Differential x-ray phase contrast imaging using a shearing interferometer," Appl. Phys. Lett. 81, 3287-3289 (2002).

[9] Momose, A., Kawamoto, S., Koyama, I., Hamaishi, Y., Takai, K. and Suzuki, Y., "Demonstration of X-Ray Talbot interferometry," Jpn. J. Appl. Phys., Part 2 42(7B), 866-868 (2003).

[10] Weitkamp, T., Diaz, A., David, C., Pfeiffer, F., Stampanoni, M., Cloetens, P. and Ziegler, E., "X-ray phase imaging with a grating interferometer," Opt. Express 13(16), 6296-6304 (2005).

[11] Pfeiffer, F., Kottler, C., Bunk, O. and David, C., "Hard X-ray phase tomography with low-brilliance sources," Phys. Rev. Lett. 98(10), 108105 (2007).

[12] Pfeiffer, F., Grünzweig, C., Bunk, O., Frei, G., Lehmann, E. and David, C., "Neutron phase imaging and tomography," Phys. Rev. Lett. 96(21), 215505-1 - 215505-4 (2006).

[13] Weitkamp, T., Tafforeau, P., Boller, E., Cloetens, P., Valade, J.-P., Bernard, P., Peyrin, F., Ludwig, W., Helfen, L. and Baruchel, J., "Status and evolution of the ESRF beamline ID19," AIP Conf. Proc. 1221, 33-38 (2010).

[14] David, C., Bruder, J., Rohbeck, T., Grünzweig, C., Kottler, C., Diaz, A., Bunk, O. and Pfeiffer, F., "Fabrication of diffraction gratings for hard X-ray phase contrast imaging," Microel. Eng. 84, 1172-1177 (2007).

[15] Weitkamp, T., David, C., Kottler, C., Bunk, O. and Pfeiffer, F., "Tomography with grating interferometers at low-brilliance sources " Proc. SPIE 6318, 63180S (2006).

[16] Müller, B., Bernhardt, R., Weitkamp, T., Beckmann, F., Brauere, R., Schurigt, U., Schrott-Fischer, A., Glueckert, R., Ney, M., Beleites, T., Jolly, C. and Schamweber, D., "Morphology of bony tissues and implants uncovered by high-resolution tomographic imaging," Int. J. Mater. Res. 98(7), 613-621 (2007).

[17] Faris, G.W. and Byer, R.L., "Three-dimensional beam-deflection optical tomography of a supersonic jet," Appl. Opt. 27, 5202-5212 (1988).

[18] Pfeiffer, F., Bunk, O., Kottler, C. and David, C., "Tomographic reconstruction of three-dimensional objects from hard X-ray differential phase contrast projection images," Nucl. Instrum. Methods Phys. Res. 580(2), 925-928 (2007).

[19] Andronache, A., von Siebenthal, M., Székely, G. and Cattin, P., "Non-rigid registration of multi-modal images using both mutual information and cross-correlation," Med. Image Anal. 12(1), 3-15 (2008).

[20] Fierz, F.C., Beckmann, F., Huser, M., Irsen, S.H., Leukers, B., Witte, F., Degistirici, Ö., Andronache, A., Thie, M. and Müller, B., "The morphology of anisotropic 3D-printed hydroxyapatite scaffolds," Biomaterials 29(28), 3799-3806 (2008).

[21] Viola, P. and Wells, W.M. "Alignment by maximization of mutual information," Proc. 5th Int. Conf. on Comp. Vis.16-23 (1995).

[22] Maes, F., Collignon, A., Vandermeulen, D., Marchal, G. and Suetens, P. "Multi-modality image registration by maximization of mutual information," Proc. IEEE Math. Meth. in Biomed. Im. Anal.14-22 (1996).